Acta Geochim (2019) 38(5):734–752
https://doi.org/10.1007/s11631-019-00318-0

ORIGINAL ARTICLE

Geochemical characterization of Granitoids in Katchuan Irruan area: further evidence for peraluminous and shoshonitic compositions and post-collisional setting of granitic rocks in the Precambrian Basement Complex of Nigeria

Chinedu U. Ibe[1] · **Smart C. Obiora**[1]

Received: 15 June 2018 / Revised: 21 December 2018 / Accepted: 10 January 2019 / Published online: 19 January 2019

Abstract Petrographic studies on Granitoids from Katchuan Irruan and adjoining areas, southeastern Nigeria, has shown that they are garnetiferous biotite granite, aplitic granite, porphyritic hornblende biotite granite, porphyritic muscovite biotite granite, weakly foliated leucogranodiorite and simple pegmatite. They are closely associated with the Precambrian Basement Complex rocks which they intruded. Modal analysis shows that the rocks consist of quartz (10%–25%), oligoclase (10%–30%), K-feldspar (15%–35%), biotite (3%–25%), with occasional garnet, hornblende, muscovite, and accessory chlorite, haematite and magnetite. Geochemical data indicates that the rocks are generally shoshonitic, alkali-calcic to calcic, ferroan and peraluminous. They are enriched in large ion lithophile elements as well as high field strength elements (Hf, Ta, Yb, Sm, Zr and Y). Their trace elements and REE patterns are similar, indicating that they are co-genetic. They are characterized by high fractionation factor (La/Yb)N (3.04–228.44) and pronounced negative Eu anomalies (Eu/Eu*) (0.23–0.71). Their overall geochemical features indicate that they were most likely derived from partial melting of crustal materials in an orogenic (post-collisional) tectonic setting. They are therefore related to the Pan-African granites, otherwise known as the Older Granites which were emplaced during the Pan African orogenic event.

✉ Chinedu U. Ibe
chinedu.ibe@unn.edu.ng

Smart C. Obiora
smartobiora@gmail.com

[1] Department of Geology, University of Nigeria, Nsukka, Nigeria

Keywords Pan African · Partial melting · Post-collisional · Precambrian · Older Granites · Orogenic

1 Introduction

Pan-African tectonics and crustal evolution have been the subject of much discussion during the last 30 years. The Nigerian Precambrian Basement Complex, which resulted from the referred tectonics is made up of three major petrological units: (1) migmatitic banded gneisses and migmatites, (2) weakly migmatized to unmigmatized paraschists also referred to as "Younger Metasediments" or "Schist belts", and (3) the Older Granite suite comprising mainly granites/granitoids, granodiorites, charnockites (hypersthene granites), syenites, as well as minor gabbroic and dioritic rocks. Unmetamorphosed dolerite and rhyolite porphyry dykes, pegmatite dykes, and numerous veins of quartzo-feldspathic composition are intrusions commonly found in the Basement Complex (Oyawoye 1964; Rahaman 1976; Makanjuola 1982; Ekwueme 1987, 1994; Olarewaju 1987; Obiora 2005, 2006).

The Precambrian Basement Complex rocks in the study area have received little attention from researchers as evidenced in the literature. Much of the information on the geology of the area is contained in geological maps of Nigeria produced by the Nigerian Geological Survey Agency where it is shown to be underlain by "Undifferentiated Basement," "Granulites Terrain," and "Granitoids" (NGSA 1994, 2004, 2011). The present study was therefore needed for the mapping and delineation of the different varieties of granitic rocks within the Precambrian Basement Complex in the area, as well as to perform detailed petrographic and geochemical studies (major-, trace-, and rare-earth elements, REEs) on the rocks for their proper classification and assessment of their petrogenesis and tectonic origin.

2 Regional geological setting

The study area is located within the extension of the Bamenda Highlands of Cameroun into southeastern Nigeria, otherwise referred to as the Bamenda Massif. The Bamenda massif constitutes the southeastern Nigerian Precambrian Basement Complex. The Precambrian Basement Complex of Nigeria belongs to the Pan-African trans-Saharan belt which is located east of the West African craton and northwest of the Congo-Gabon craton. Based on evidence from the eastern and northeastern margins of the West African craton, it has been observed by previous authors that the Pan-African trans-Saharan belt evolved by plate tectonic processes which involved the collision of the active margin of the Pharusian belt (Taureg shield) and the passive continental margin of the West African craton, about 600 Ma (Fig. 1, Burke and Dewey 1972; Leblanc 1981; Black et al. 1979; Caby et al. 1981). Subduction and consequent collision at the eastern margin of the West African craton (McCurry and Wright 1977) produced extensive melting of the older rock suites resulting in the emplacement of the mainly calc-alkaline granitoids and basaltic intrusions.

High positive gravity anomaly, which occurs in a narrow zone within the Dahomeyide orogen located at the southeastern margin of the West African craton in Togo and Benin Republic, is evidence of evolution by plate tectonic processes involving the collision of the Pharusian belt and the West African craton (Obiora 2012). The collision at this plate margin is believed to have led to the reactivation and remobilization of the internal region of the Pan-African belt. The Nigerian Precambrian Basement Complex lies within the remobilized part of the belt.

The Nigerian Precambrian Basement Complex rocks are also believed to be the results of at least four major orogenic cycles of deformation, metamorphism, reactivation, and remobilization corresponding to the Liberian (2650 ± 150 Ma), the Eburnean (2000 ± 50 Ma), the Kibaran (1100 ± 200 Ma), and the Pan-African cycles (600 ± 150 Ma). Using the International Geologic Time Scale (2002), these ages can be referred to as, Paleoarchean to Mesoproterozoic (3600 to 1600 Ma) for Liberian and Eburnean, Mesoproterozoic to Neoproterozoic (1600 to 1000 Ma) for Kibaran, and Neoproterozoic to Early Paleozoic (1000 to 545 Ma) for Pan-African.

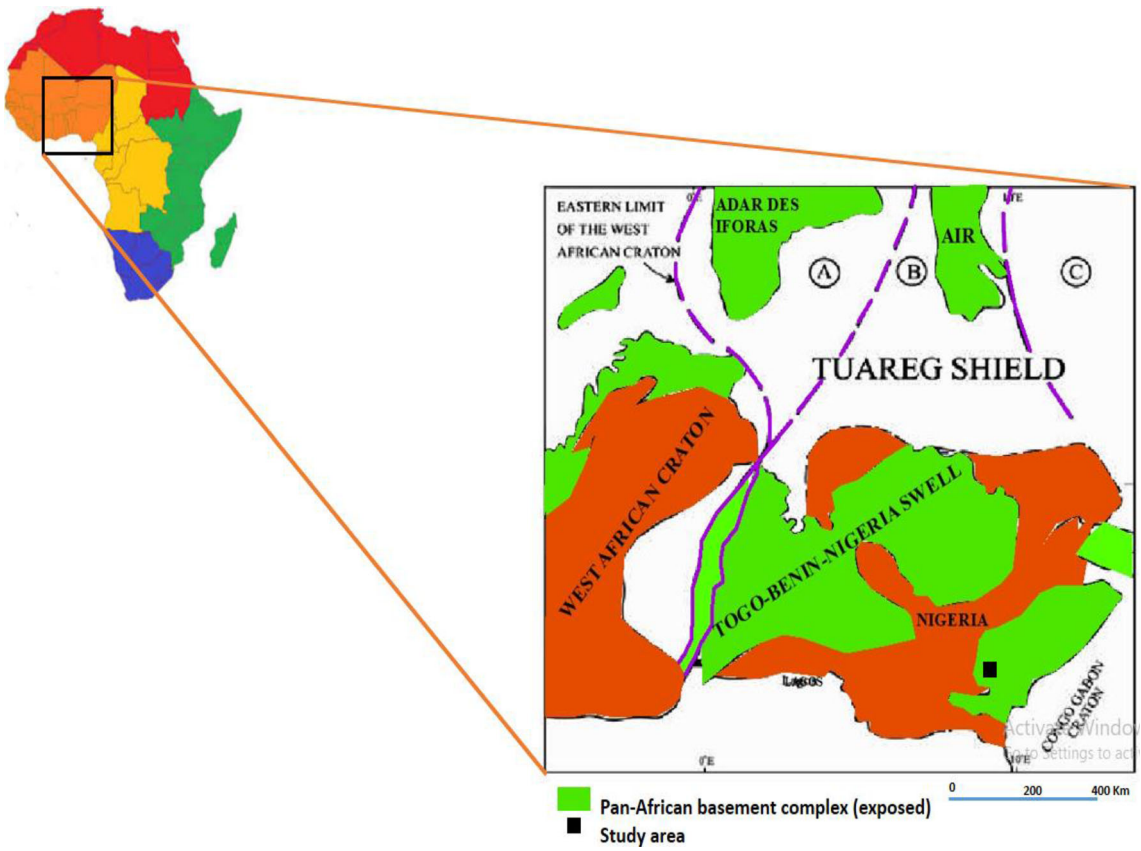

Fig. 1 The location of the Precambrian Basement Complex in Nigeria between the West African craton, the Congo-Gabon craton and the southern part of the Tuareg shield (after Obiora 2012). **a** Western part of the Tuareg shield called the Pharusian belt; **b** central part (the Hoggar-Air segment) and **c** eastern part (the East-Saharan craton)

Three major lithological units recognized within the Nigerian Precambrian Basement Complex include:

1. Migmatite-gneiss complexes, which is comprised of biotite and biotite hornblende gneisses, quartzites and quartz schist, and small lenses of calc-silicate rocks.
2. Slightly migmatized to unmigmatized paraschists and metaigneous rocks which consist of pelitic schists, quartzites, amphibolites, talcose rocks, metaconglomerates, marbles, and calc silicate rocks.
3. Older Granites which is comprised of rocks varying in compositions from granodiorites to granites and potassic syenite (Akoh et al. 2015).

The Pan-African (Older) granite suite includes porphyritic/porphyroblastic muscovite granites, aplites, granodiorites, diorites, quartz-hypersthene diorites, and charnockites (Obiora 2005). They are often weakly foliated and described as foliated granites and gneissic granites. Contacts of these Older granites with other rocks of the Precambrian Basement Complex are characteristically gradational suggesting a non-magmatic origin, possibly emplaced during the last of the reactivation events that affected the Basement Complex, i.e. during deformation and metamorphism of the supracrustals (Pan-African orogeny) (Rahaman 1976). The Pan-African granites are medium to coarse-grained, containing both muscovite and biotite, plagioclase (An_6–An_{15}), and microcline. Petrographically and geochemically, the Older Granites are calc-alkaline and peraluminous with high K_2O contents and numerous K-feldspar porphyroblasts, which relates them to widespread basement rejuvenation during the Pan-African thermotectonic event (Oyawoye 1970).

Neoproterozoic to Early Paleozoic ages (638–510 Ma) from U–Pb, Rb–Sr, K–Ar dating methods on zircon have been reported for granitoids within the Nigerian Schist belt areas (Grant 1978; Caen-Vachette and Umeji 1983). On the basis of mineralogy and texture as well as field relationships, Jones and Hockey (1964) have recognized three phases of the Older Granite suite; an early phase comprising closely intermingled gabbroic rock, granodiorites and quartz diorites, and dolerites, the main phase, which comprises coarse porphyritic hornblende granite, coarse porphyritic biotite granite, syenite, and a late phase comprising homogenous granite, pegmatite, and aplite dykes. Because of field and geochemical evidence, however, Rahaman (1989), Dada and Respaut (1989), Dada et al. (1995), Ferre et al. (1998, 2002) have refuted the retention of dolerite as integral part of the early phase granites as reported by Jones and Hockey (1964) (Table 1). These authors are of the opinion that the unmetamorphosed doleritic rock, which cross-cuts the granitoids (granites, granodiorites, charnockites), is the youngest of the Nigerian Basement Complex rocks (Akoh et al. 2015).

3 Field occurrence and petrography of the granitoids

The granitoids in this study occur mainly in the Ukpe–Bawop, Idum–Aragban, and Katchuan–Okundi axes where they intruded migmatitic gneisses (Fig. 2). The details of

Table 1 Details of samples of the granitic intrusions and their locations

Sample No.	Location No. (Fig. 2)	Location name	Name of rock
1PAG	IBE-1	Ekumtak	Porphyritic Aplitic Granite
2PAG	IBE-1	-do-	
3PAG	IBE-8	Kakwagom	
4PAG	IBE-8	-do-	
1PBMG	IBE-7	Ukpe	Porphyritic Biotite Muscovite Granite
2PBMG	IBE-4	Ekumtak	
3PBMG	IBE-10	Katchuan Irruan	
4PBMG	IBE-25	Aragban	
1PBHG	IBE-7	Ukpe–Bawop road	Porphyritic Biotite Hornblende Granite
2PBHG	IBE-15	Bawop–Katchuan road	
3PBHG	IBE-16	Bitsha	
1WFL	IBE-9	Elem–Elem stream, Katchuan Irruan	Weakly foliated Leucogranodiorite
2WFL	-do-		
3WFL	-do-		
1GBG	IBE-2	Ukwelishegbe hills, Ekumtak	Garnetiferous Biotite Granite
2GBG	-do-		
1SP	IBE-6	Ukpe–Bawop road	Simple Pegmatite

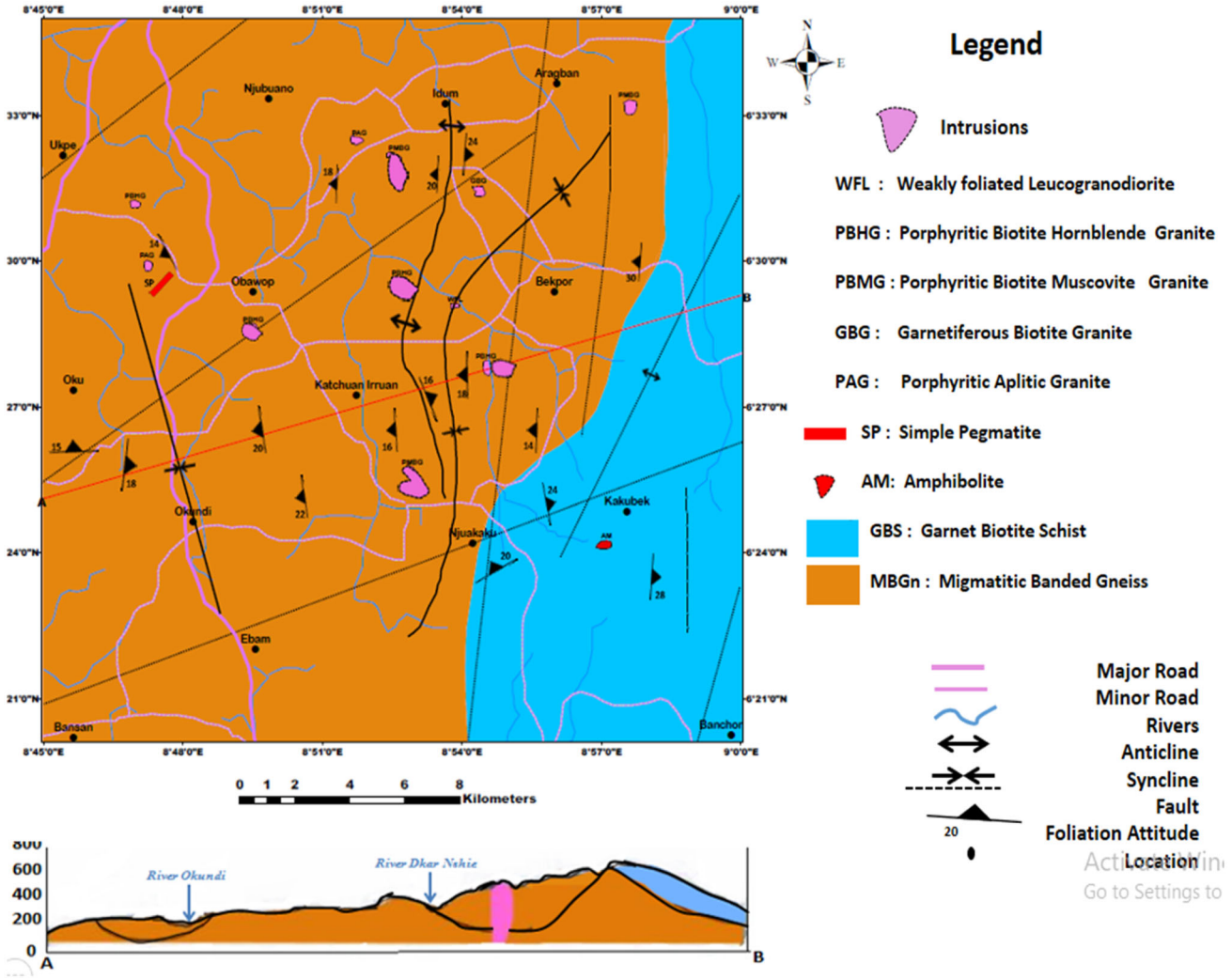

Fig. 2 Geological map of the study area

the samples of the granitic intrusions and their locations are shown in Table 1 and the estimated modal compositions of the granitic rocks in the study area (values in %) is presented in Table 2.

3.1 Garnetiferous biotite granite (GBG)

The rock is leucocratic, coarse-grained, and porphyritic, with phenocrysts of garnet, set in a medium to coarse-grained, equigranular groundmass with the ratio of phenocryst to groundmass at about 1:4. The groundmass consists of interlocking crystals of biotite, feldspar, and quartz. Lots of cross-cutting quartzo-feldspathic veins characterize the outcrop. Garnet measuring about 5 mm occurs in somewhat rounded crystals riddled with inclusions of quartz, biotite, and plagioclase optically identified as Oligoclase (An_{12}).

3.2 Porphyritic aplitic granite (PAG)

The rock is fairly leucocratic, medium-grained, and porphyritic, with a sugary texture. It consists of phenocrysts of feldspar and quartz in a groundmass of the same minerals as well as biotite and muscovite. It consists of plagioclase megacrysts embedded in an aplitic groundmass. The plagioclase megacrysts which constitute about 24% volume and measure about 8 mm are characterized by combined albite-Carlsbad twinning and contains inclusions of muscovite, biotite, and opaques (Fig. 3c). The groundmass is fine-grained, containing an equigranular mosaic of quartz, albite, biotite, and secondary muscovite resulting from the alteration of biotite. The quartz crystals, 2 to 3 mm in diameter, are mostly anhedral showing strong undulatory extinction.

The subhedral plagioclase grains are sericitized, and for this reason, the optical measurements of the anorthite

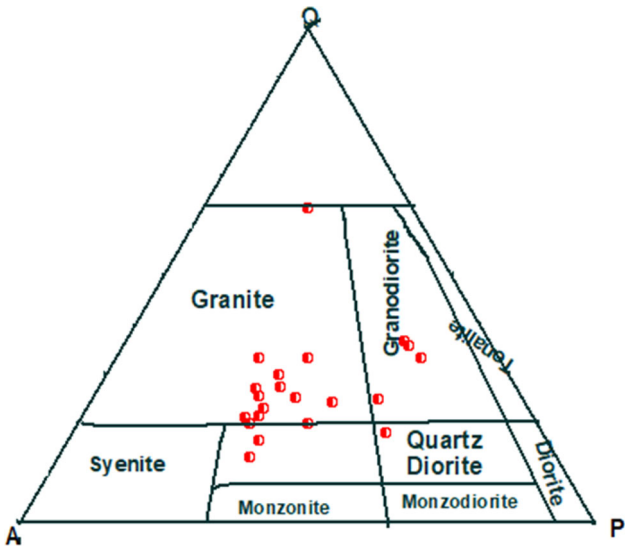

Fig. 3 Plot of the average modal compositions of the granitic rocks on the Quartz-Alkali Feldspar-Plagioclase (QAP) classification diagram (after Strekeisen 1976)

content are uncertain. Accessory minerals in the rock include apatite, ilmenite, zircon, and magnetite. Biotite occurs as laths and shows pleochroic haloes resulting from radioactive damage caused by zircon.

3.3 Weakly foliated leucogranodiorite (WFL)

The rock is leucocratic and medium grained. The minerals present in the rock include quartz, plagioclase, and biotite. The rock is weakly foliated as shown by weak alignment of biotite in a preferred direction. The phenocrysts are made up of subhedral to anhedral crystals of oligoclase, set in a medium-grained groundmass of quartz, biotite, and oligoclase. Some of the phenocrysts have been sericitized. They measure about 5 mm and make up about 22% of the total rock volume. The foliation is shown by the subparallel arrangement of biotite, stretched quartz and oligoclase. The quartz crystals measure about 1 to 2 mm. Some of the crystals which exhibit undulose extinction occur as inclusions in the plagioclase phenocrysts. Plagioclase, which is oligoclase (An_{13}), occurs in rectangular shaped, subhedral crystals. The biotite is brown in color and strongly pleochroic from light brown to dark brown and lath-shaped. The accessory minerals include primary hematite, magnetite, and ilmenite.

3.4 Porphyritic biotite muscovite granite (PBMG)

The rock is leucocratic, coarse-grained, and porphyritic. The phenocrysts consist of plagioclase and K-feldspars in a coarse-grained groundmass of quartz, K-feldspars, and biotite. Dimensions of the phenocrysts range from 2.4 to 5.0 cm by 1.0 to 2.4 cm. Some occur within the migmatitic banded biotite gneiss, the porphyroblastic garnet cordierite sillimanite gneiss, and the garnet mica schist while others just occur isolated as boulders. The phenocrysts consist of microcline and quartz, which are set in a coarse-grained groundmass of muscovite, biotite, quartz, and plagioclase (Fig. 3b). The accessory minerals include chlorite which replaces biotite at the rim and along cleavages, magnetite, and hematite replacing primary magnetite.

The phenocrysts of microcline range from 2 to 5 mm long and consist of either a single crystal or a mosaic of crystals. They frequently contain inclusions of plagioclase and minor amounts of the accessory minerals. Some of the plagioclase inclusions (An_{10}) are euhedral, some are sericitized. Muscovite which measures about 4 mm is platy and subhedral and shows some degree of alteration.

3.5 Porphyritic biotite hornblende granite (PBHG)

The rock is leucocratic, coarse grained, and shows the very weak alignment of the mafic minerals (biotite and hornblende). The rock is distinctly porphyritic, with phenocrysts of well-formed, plagioclase and K-feldspars embedded in a groundmass of quartz, biotite, and hornblende. The rock mainly occurs as in situ boulders. Microcline phenocrysts are characterized by cross-hatched twinning and measure up to 8 mm. Hornblende occurs in subhedral elongate sections. It measures up to 6 mm (Fig. 3a).

3.6 Simple pegmatites (SP)

The rock is leucocratic and extremely coarse-grained. Its constituent minerals are mainly plagioclase (4 cm), biotite (3 cm) and quartz (3 cm). The pegmatite outcrop is restricted to the WNW part of the study area where it occurs in association with the porphyritic aplitic granite and the porphyroblastic garnet cordierite sillimanite gneiss host rock. Its total length is about 0.5 km with a width of about 20 m.

4 Sampling and analytical method

Seventeen (17) fresh representative samples consisting of 2 garnetiferous biotite granite (GBG), 4 porphyritic muscovite biotite granite (PMBG), 3 porphyritic hornblende biotite granite (PHBG), 3 weakly foliated leucogranodiorite (WFL), 4 porphyritic aplitic granite (PAG), and 1 simple pegmatite (SP) were selected for geochemical analysis. The samples were crushed in a jaw crusher at the Inorganic Geochemistry Research Laboratory of the Department of Geology, University of Nigeria, Nsukka.

Table 2 Estimated modal compositions of the granitic rocks in the study area (values in %)

	1PAG 1	2PAG 2	3PAG 3	4PAG 4	PAGav	1PBMG 5	2PBMG 6	3PBMG 7	4PBMG 8	PBMGav	1PBHG 9
Quartz	15	10	10	20	14	10	10	15	20	14	15
Microcline	15	25	15	20	19	40	30	30	25	31	35
Orthoclase	20	25	20	5	18						
Plagioclase	30	15	30	20	24	25	20	20	15	20	20
Biotite	10	15	15	20	15	5	10	10	15	10	15
Hornblende											10
Garnet											
Muscovite						10	15	15	20	15	5
Chlorite	5		5	5	3	5	10		5	7	
Haematite						3	2	5			
Magnetite	5	10	5			2	3	5			
Zircon											
Total	100	100	100	100		100	100	100	100		100

	2PBHG 10	3PBHG 11	PBHGav	1WFL 12	2WFL 13	3WFL 14	WFLav	1GBG 15	2GBG 16	GBGav	SP 17
Quartz	20	15	17	25	25	25	25	15	10	13	35
Microcline	30	25	30	10	10	10	10	20	20	20	10
Orthoclase				10							
Plagioclase	23	15	19	40	35	35	33	15	20	18	10
Biotite	10	15	13	5	3	10	9	25	20	23	40
Hornblende	10	25	15								
Garnet					10			20	20	20	
Muscovite	5		3								
Chlorite					2						
Haematite					5	7			5		
Magnetite	2	3		10	5	13		5	5		5
Zircon					5						
Total	100	100		100	100	100		100	100		100

The crushed samples were pulverized in a Vibrating Disc Mill. Final size reduction, mixing, and homogenization to < 75 μm were done with a Mixer Mill. One hundred gram (100 g) of each sample were thereafter packaged and dispatched to Bureau Veritas Minerals Pty Ltd., Canning Vale, Perth, Western Australia for major element oxides and trace element geochemistry using an X-ray fluorescence (XRF) and inductively coupled mass spectrometry (ICP-MS), respectively.

The samples were fused with sodium peroxide and subsequently, the melt was dissolved in dilute hydrochloric acid for analysis. Boron was determined by inductively coupled plasma-optical emission spectrometry (ICP-OES).

The samples were cast using a 66:34 flux with 4% lithium nitrate added to form a glass bead. The major elements were determined by X-ray fluorescence spectrometry (XRF) except for FeO which was determined volumetrically.

Trace elements were determined by laser ablation inductively coupled plasma mass spectrometry (LA-ICPMS). Loss on ignition (LOI) result was determined using a robotic thermogravimetric analyzer (TGA) system. Furnaces in the system were set to 110 and 1000 °C.

5 Results

5.1 Major elements

The major element oxides data, with CIPW norms on the rocks, are presented in Table 3. Some important variables, including Fe-number (Fe*), Aluminium Saturation Index (ASI or A/CNK), and Modified Alkali-Lime Index (MALI

Table 3 Major element oxide (wt%) compositions of granitic rocks from Katchuan Irruan and adjoining areas

	1PAG	2PAG	3PAG	4PAG	1PMBG	2PMBG	3PMBG	4PMBG
SiO_2	64.55	68.06	69.76	67.59	70.43	73.39	64.98	67.64
TiO_2	1.36	0.91	0.66	0.85	0.48	0.15	1.29	1
Al_2O_3	15.1	14.6	14.6	14.9	13.7	14.2	15.1	14.8
Fe_2O_3	5.71	4.26	2.97	4.04	3.83	1.33	5.47	4.51
MnO	0.07	0.05	0.04	0.05	0.04	0.02	0.07	0.05
MgO	1.25	0.83	0.61	0.8	0.42	0.32	1.21	0.17
CaO	2.82	1.6	1.46	1.91	1.43	0.61	2.7	2.01
Na_2O	3.16	2.79	2.93	2.89	2.36	2.58	3.09	3.09
K_2O	4.68	5.53	5.85	5.8	6.04	6.58	6.86	4.99
P_2O_5	0.55	0.35	0.21	0.33	0.17	0.1	0.52	0.35
LOI	0.28	0.35	0.34	0.43	0.72	0.38	0.21	0.34
Total	99.52	99.33	99.43	99.60	99.62	99.66	101.5	98.95
$K_2O + Na_2O$	7.84	8.32	8.78	8.69	8.4	9.16	9.95	8.08
A/NK	1.93	1.75	1.66	1.71	1.63	1.55	1.52	1.83
A/CNK	1.42	1.47	1.43	1.41	1.39	1.45	1.19	1.47
CNK	10.66	9.92	10.24	10.6	9.83	9.77	12.65	10.09
A-C	5.02	6.72	7.32	6.78	6.97	8.55	7.25	6.07
F/K	2.18	1.39	0.88	1.20	1.13	0.32	1.45	1.53
Log F/K	0.34	0.14	-0.05	0.08	0.05	-0.48	0.16	0.19
S/A	4.27	4.66	4.78	4.54	5.14	5.17	4.30	4.57
Log S/A	0.63	0.67	0.68	0.66	0.71	0.71	0.63	0.66
P_2O_5/TiO_2	0.40	0.38	0.32	0.38	0.35	0.67	0.40	0.35
MgO/CaO	0.44	0.52	0.42	0.42	0.29	0.52	0.45	0.08
CIPW norm								
Q	21.6	26.4	26.7	23.6	29.4	31.4	14.4	26.5
Or	27.8	32.9	34.8	34	35.5	38.6	40.3	29.4
Ab	26.9	23.7	29.4	24.3	29.4	21.68	25.96	26
An	10.5	6	6.3	7.6	6.2	2.4	7	8.05
C	1	1.9	1.2	1.1	1	1.95		1.34
Di wo							1	
Di en							1.4	
Hy en	4.6	3.5	2.1	2.7	2.6	0.95	3.5	0.9
mt	8.3	6.2	4.3	5.8	5.5	1.9	7.9	6.5
Il	2.6	1.7	1.3	1.6	0.9	0.28	2.4	1.9
he								
ap	1.2	0.8	0.5	0.7	0.4	0.2	1.1	0.77

	1PBHG	2PBHG	1WFL	2WFL	3PBHG	3WFL	1GBG	2GBG	1SP
SiO_2	70.84	72.89	66.09	67.86	63.19	74.87	71.11	60.86	77.18
TiO_2	0.53	0.13	1.1	0.42	0.85	3.07	0.6	0.9	0.02
Al_2O_3	13.9	14.5	15.1	15.7	16	14.5	14.9	17.5	13.6
Fe_2O_3	3.28	1.17	4.68	3.86	7.02	0.79	2.82	8.62	0.96
MnO	0.04	0.02	0.06	0.06	0.13	0.01	0.03	0.15	0.1
MgO	0.53	0.29	1.1	1.76	3.66	0.14	1.35	4.31	0.08
CaO	0.8	0.82	2.18	4.17	3	1.26	3.07	1.51	1.67
Na_2O	2.6	2.85	3.02	3.88	2.86	3.97	3.62	1.9	4.7
K_2O	5.96	6.65	5.16	1.81	2.5	3.79	1.38	2.64	1.43
P_2O_5	0.2	0.76	0.365	0.13	0.22	0.03	0.07	0.19	0.03
LOI	0.8	0.39	0.42	0.18	0.57	0.44	0.63	1.18	0.28

Table 3 continued

	1PBHG	2PBHG	1WFL	2WFL	3PBHG	3WFL	1GBG	2GBG	1SP
Total	99.48	100.47	99.27	99.83	100	102.87	99.58	99.81	100
$K_2O + Na_2O$	8.56	9.5	8.18	5.69	5.36	7.76	5	4.54	6.13
A/NK	1.62	1.52	1.84	2.75	2.98	1.86	2.98	3.85	2.21
A/CNK	1.48	1.40	1.45	1.59	1.91	1.60	1.84	2.89	1.74
CNK	9.36	10.32	10.36	9.86	8.36	9.02	8.07	6.05	7.8
A-C	7.76	8.68	6	1.52	2.36	6.5	1.93	3.03	4.46
F/K	0.96	0.27	1.53	3.45	4.99	0.30	3.59	3.31	1.06
Log F/K	-0.01	-0.55	0.18	0.53	0.69	-0.52	0.55	0.52	0.02
S/A	5.09	5.02	4.37	4.32	3.94	5.16	4.77	3.47	5.67
Log S/A	0.70	0.70	0.64	0.63	0.59	0.71	0.67	0.54	0.75
P_2O_5/TiO_2	0.37	5.84	0.33	0.31	0.26	0.01	0.11	0.21	1.65
MgO/CaO	0.66	0.35	0.50	0.42	1.22	0.11	0.43	2.85	0.04
CIPW norm									
Q	29.5	30.6	23	26.7	24.2	34.2	36.1	32.5	40.4
Or	35	39.1	30.3	10.6	14.7	22.3	8.1	15.5	8.4
Ab	21.9	23.9	25.3	32.6	24	33.3	30	13.01	39.4
An	2.9	-0.7	8.8	19.9	13.4	6.2	14.8	6.3	8.1
C	2.1	2.9	1.3	0.05	3.6	1.6	2.1	9.8	
Di wo									
Di en									
Hy en	3.8	0.8	3.12	5	12.2	0.4	4	10.7	0.6
mt	4.7	1.7	6.8	5.6	10.1		4.1		1.4
Il	1	0.3	2.1	0.8	1.2	0.8	1.1	0.6	0.04
he									
ap	0.4	1.7	0.8	0.3	0.5	0.1	0.2	0.4	0.07

or N + K-Ca) proposed by Frost et al. (2001) have been computed and included in Table 3. The granitic rocks are generally hypersthene and corundum-normative. They have SiO_2 (60.86% to 77.18%), Al_2O_3 (13.6% to 17.5%), Fe* (1.14% to 12.49%) and alkali ($Na_2O + K_2O$) (4.54% to 9.95%) contents.

5.2 Trace and rare-earth elements

Trace element compositions (ppm) of the granitic rocks, which are of petrogenetic significance, are presented in Table 4. The data is plotted on the Harker variation diagram (Fig. 14) and the rocks show calc-alkaline trends with Sr, Ba, La, Zr, and Nb decreasing and Rb increasing but almost scattered with increasing SiO_2. Trace element data on the rocks from the study area have been normalized to chondrites after Thompson (1982) and plotted as a spidergram (Fig. 4). The rocks show an overall enrichment of the large ion lithophile elements (LILE: K, Th, Ba, and Rb). HFS elements usually occur in accessory minerals such as rutile and zircon. The samples are relatively enriched in Zr, Hf, and Nb (Table 4) indicating the presence of accessory minerals in the rocks.

They also show strong positive anomalies in Th, K, La, Ce, Nd, Sm, and Tb and negative anomalies in Ba, Nb, Ta, Sr, Zr, and Ti. It also shows a high concentration of W and Co which resulted from the vibratory tungsten carbide (WC) disc mill used in preparing the samples but there were no Ca, Ta, and Sc contaminations as expected.

The rare-earth elements compositions (ppm) of the rocks are presented in Table 4.

Figure 5 shows the chondrite-normalized REE (Rare Earth Elements) patterns using the values of Sun and McDonough (1991).

The granitic rocks exhibit similar REE patterns exhibiting LREE enrichment relative to MREE and HREE, with distinct negative Eu-anomalies (Eu/Eu* = 0.23–0.71), inclined MREE and flat HREE. The fractionated, La_N/Yb_N ratios in the granitic rocks range from 3.04 to 28.4 (Fig. 6).

Table 4 Trace and rare-earth elements compositions (ppm) of the granitic rocks from Katchuan Irruan and adjoining areas

	1PAG	2PAG	3PAG	4PAG	1PBMG	2PBMG	3PBMG	4PBMG
Sc	7.6	4.3	23.3	6	4.3	1.1	6.5	4.4
V	39.3	26.1	24.7	27.7	9.2	3	39.5	36
Cr	14	7	38	7	8	0	17	18
Co	46.7	15.6	23.5	25.1	21.1	8.3	20.3	23.4
Ni	20	6	6	6	6	1	10	12
Cu	22	16	42	24	18	4	22	16
Zn	125	95	95	115	90	45	135	110
Ga	21.5	19.6	19.7	21.8	21.9	15.6	24.9	22.9
Rb	213	242	208	261	199	181	215	206
Sr	410	258	268	277	152	149	398	438
Y	24.9	17.8	12	18.7	17.3	8.44	24.6	16.7
Zr	909	753	478	725	470	116	918	741
Nb	37.7	31.1	21	32.1	31.7	11.6	37.3	28.3
Sn	1.8	1.2	2	1.6	1.4	1.2	1.8	2.2
Sb	0.2	0.3	0.3	0.4	0	0.2	0.5	0.2
Cs	2.76	0.75	0.68	1.02	1.37	1.68	0.8	1.59
Ba	1710	1530	1640	1700	860	926	1780	1910
Hf	22.8	19.4	14.3	18	14.3	3.99	22	16.6
Ta	3	1.54	2.14	1.88	1.11	0.63	1.96	1.61
W	1010	221	346	486	237	155	220	285
Tl	1	1.2	1.2	1.2	1	1	1.2	1.2
Pb	22	25	35	33	26	35	25	25
Th	55.3	35.1	50.5	80.8	53.1	30.4	51.8	47.8
U	2.23	1.21	1.27	2.1	1.85	2.69	2.77	1.68
Ga	21.5	19.6	19.7	21.8	21.9	15.6	24.9	22.9
Y + Nb	62.6	48.9	33	50.8	49	20.04	61.9	45
La	239	159	225	293	215	61.6	233	197
Ce	461	320	381	578	406	126	452	371
Pr	54.3	37.8	50.2	69.7	49.3	14.9	54	40.1
Nd	175	129	170	220	168	51.5	183	132
Sm	21.3	17.3	19.4	29.9	27.3	9.68	24	17.1
Eu	2.39	1.68	1.83	2.18	1.4	1.06	2.55	2.08
Gd	11.7	8.57	7.64	12.11	12.6	5.22	10.8	7.37
Tb	1.29	0.98	0.87	1.2	1.49	0.64	1.26	0.94
Dy	5.91	4.13	3.25	4.82	4.93	2.44	5.48	3.92
Ho	0.91	0.67	0.57	0.7	0.76	0.33	0.88	0.51
Er	1.94	1.48	1.1	1.79	1.65	0.55	2.17	1.23
Tm	0.22	0.2	0.18	0.16	0.19	0.06	0.29	0.17
Yb	1.43	0.98	0.48	0.92	0.84	0.31	1.55	0.92
Lu	0.16	0.13	0.11	0.11	0.11	0.04	0.16	0.15
$\sum$REE	976.55	681.92	861.63	1214.59	889.57	274.33	971.1	774.49
$\sum$LREE	950.6	663.1	845.6	1190.6	865.6	263.68	946	757.2
$\sum$HREE	23.56	17.14	14.2	21.81	22.57	9.59	22.59	15.21
$\sum$LR/HR	40.34	38.68	59.54	54.58	38.35	27.49	41.87	49.78
LA_N/Yb_N	119.88	116.37	336.23	228.44	183.59	142.53	107.8	153.59
Ce_N/Yb_N	89.54	90.7	220.48	174.51	134.25	112.9	81	112.01
La_N/Sm_N	7.24	5.93	7.48	6.32	5.08	4.1	6.26	7.43
La_N/Lu_N	160.08	131.08	219.21	285.46	209.47	165.04	156.1	140.75
Eu/Eu*	0.46	0.42	0.45	0.35	0.23	0.45	0.48	0.56

Table 4 continued

	1PBHG	2PBHG	3PBHG	1WFL	2WFL	1GBG	3WFL	2GBG	1SP
Sc	5	1.7	7.3	18.6	0.8	1.7	22.7	0.3	3.5
V	16	3.5	60.3	145	4.8	48.7	179	0.9	44
Cr	14	3	29	113	0	25	120	0	14
Co	16.8	24.9	19.9	24.9	5.8	17	36.3	48.4	10.9
Ni	16	4	12	78	4	28	90	6	8
Cu	26	8	8	24	4	172	114	1	22
Zn	75	25	40	100	20	40	130	4	40
Ga	19.9	14.8	17.4	18.5	16.6	17.6	21.3	18.3	20.8
Rb	192	156	65.4	84.1	62.9	42.6	88.1	35.1	35.2
Sr	236	196	421	212	134	325	156	258	685
Y	26.2	22.2	9.96	33.5	6.52	8.18	37.1	30.6	8.08
Zr	507	72.9	114	184	50	196	194	56	171
Nb	27.9	7.44	4.1	9.24	3.87	9.89	9.21	1.17	1.53
Sn	2.2	1	1.2	1.8	0.8	2	1.6	0.6	0.8
Sb	0.1	0.3	0.2	0.3	0.3	0.3	0.3	0.2	0.1
Cs	0.52	0.67	1.43	4.61	0.33	2.04	4.64	0.46	0.63
Ba	1350	965	661	501	610	497	526	193	346
Hf	14.9	2.63	2.9	4.62	2.25	6.6	5.05	2.14	4.72
Ta	1.1	1.11	0.54	0.71	0.32	1.03	0.89	1.1	0.09
W	260	549	152	105	81	170	175	837	68.4
Tl	1.4	1	0.4	0.6	0.4	0.4	0.6	0.3	0.4
Pb	27	40	9	17	12	23	12	29	6
Th	48.2	20.2	4.52	5.93	6.19	10.3	8.12	3.75	0.38
U	1.49	3.09	0.78	2.08	0.68	2.66	2.86	2.54	0.23
Ga	19.9	14.8	17.4	18.5	16.6	17.6	21.3	18.3	20.8
Y + Nb	54.1	29.64	14.06	42.74	10.39	18.07	46.31	31.77	9.61
La	155	31.8	19.3	22.9	14.4	30.4	32	14.5	8.17
Ce	303	66.8	31.6	47	26.6	57.4	64.8	26.8	17.4
Pr	40.5	8.26	4.45	6.25	3.26	7.31	8.31	2.91	2.19
Nd	150	30.8	17	24.3	10.8	25.7	31.1	10.5	9.77
Sm	25.2	7.41	2.64	5.93	2.42	5.15	7.85	1.87	2.2
Eu	1.66	0.18	0.84	1.38	0.42	1.55	1.48	1.87	0.56
Gd	11.4	5.43	2	5.83	1.51	3.1	6.12	1.02	1.73
Tb	1.44	0.82	0.35	0.93	0.24	0.3	1.02	0.45	0.3
Dy	6.99	3.93	16	5.37	1.2	1.54	6.33	4.17	1.52
Ho	1.06	0.73	0.36	1.21	0.21	0.28	1.4	1.27	0.39
Er	2.08	1.88	1.02	3.3	0.6	0.44	3.46	5.42	0.81
Tm	0.28	0.2	0.21	0.55	0.06	0.1	0.53	1.12	0.09
Yb	1.37	1.44	3.38	1.08	3.39	0.47	3.48	8.63	0.32
Lu	0.14	0.18	0.16	0.45	0.05	0.52	0.36	0.46	0.07
∑REE	700.1	159.86	99.31	126.5	65.16	134.3	168.24	80.99	45.52
∑LREE	673.7	145.07	74.99	106.4	57.48	126	144.06	56.58	39.73
∑HREE	24.76	14.61	23.48	18.72	7.26	6.75	22.7	22.54	5.23
∑LR/HR	27.2	9.92	3.19	5.68	7.91	18.66	6.34	2.51	7.6
LA_N/Yb_N	81.15	15.84	4.09	15.2	3.04	46.39	6.59	1.2	18.31
Ce_N/Yb_N	61.43	12.88	2.59	12.08	2.17	33.92	5.17	0.86	15.1
La_N/Sm_N	3.97	2.77	4.71	2.49	3.84	3.81	2.63	5	2.4
La_N/Lu_N	118.7	18.93	12.92	5.45	30.86	6.26	9.52	3.37	12.51
Eu/Eu*	0.29	0.08		0.71	0.67		0.65		0.88

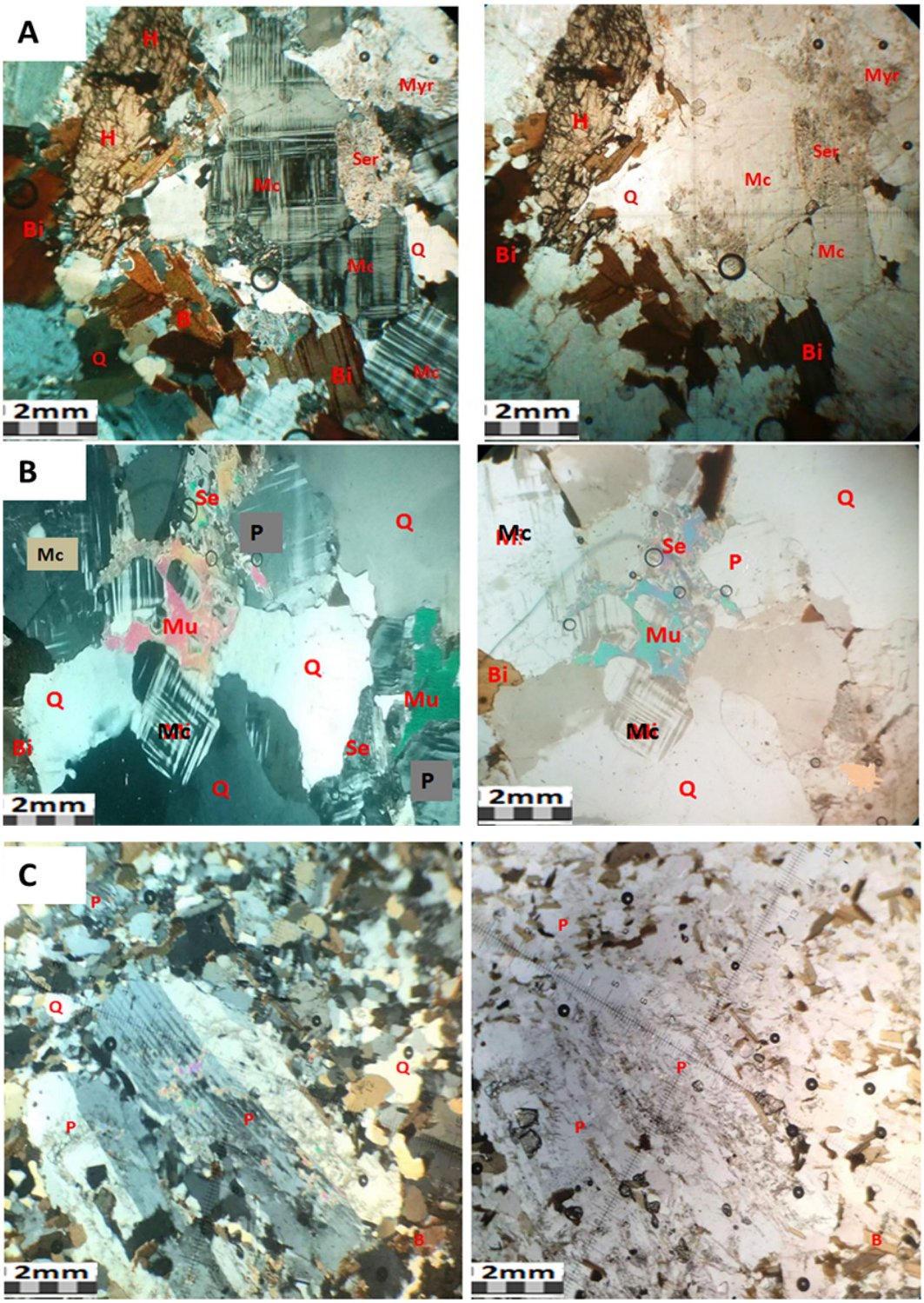

Fig. 4 **a** Photomicrograph of PHBG from location IBE-11 showing basal section of hornblende (H), microcline (Mc) phenocrysts, myrmekite (Myr), sericite (Ser), biotite (B) and quartz (Q) in crossed and plane polars (Crossed nicols; X4). **b** Photomicrograph of PMBG from location IBE-10 showing quartz (Q) and microcline (Mc) phenocrysts in cross and plane polars. **c** Photomicrograph of (PAG) from location IBE-8 showing plagioclase (P) megacryst exhibiting combined Albite-Carlsbad twinning in crossed and plane polars (Crossed nicols; ×4)

6 Discussion

6.1 Petrographic characteristics of the granite rocks

The granitoids in the Precambrian Basement Complex rocks in Katchuan Irruan and adjoining areas are garnetiferous biotite granite, porphyritic aplitic granite, porphyritic biotite muscovite granite, porphyritic biotite hornblende granite, and weakly foliated leucogranodiorite as well as simple pegmatites, representing the Older or Pan-African granite.

The granitic rocks plot mainly in the field of alkali granite on the total alkali ($Na_2O + K_2O$) versus silica, (SiO_2) (TAS) diagram of Cox et al. (1979), adapted by Wilson (1989) for the chemical classification and nomenclature of the granitic rocks (Fig. 7). This is apparently due to their high contents of K_2O. The graphical presentations of the variation of the major oxides with SiO_2 in the granitic intrusions (Harker diagrams) are shown in Fig. 8. It is observed that Al_2O_3, CaO, TiO_2, FeO(t), MgO, MnO, and P_2O_5 decrease with increasing SiO_2. K_2O displays a positive correlation with SiO_2, whereas Na_2O does not show any correlation. The scatter in the plots of Na_2O may be due to contamination and local assimilative reaction leading to inhomogeneity within the granitic rocks (Khalaji 2007).

The rocks plot mostly in the shoshonitic field of the K_2O versus SiO_2 diagram of Le Maître et al. (1989) for discrimination of subalkaline rocks, with a few of the samples plotting in the high to medium-K-calc-alkaline field (Fig. 9). The sporadic abundance of K-feldspar phenocrysts provide ample evidence for K-metasomatism.

The $Al_2O_3/(Na_2O + K_2O)$ versus $Al_2O_3/(CaO + Na_2O + K_2O)$ binary diagram (Fig. 10) has been used to discriminate peraluminous, metaluminous, and peralkaline magma series (Shand 1943). This diagram was adapted, and it reveals that the granitic rocks in this study are peraluminous.

Fig. 7 Classification of the granitic rocks using the total alkalis ▶ versus silica (TAS) diagram of Cox et al. (1979) adapted by Wilson (1989) for plutonic rocks. The curved red solid line subdivides alkaline and subalkaline rocks

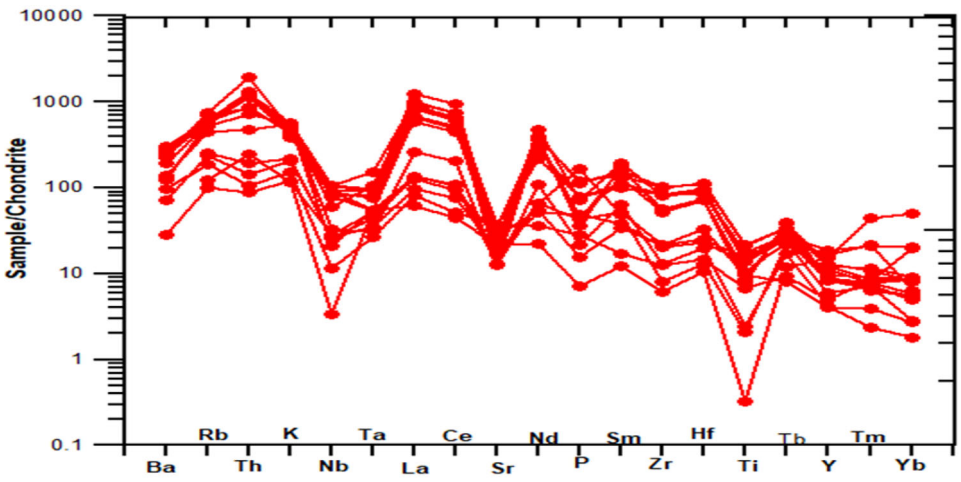

Fig. 5 Chondrite-normalized Spidergram for the granitic rocks (values from Thompson 1982)

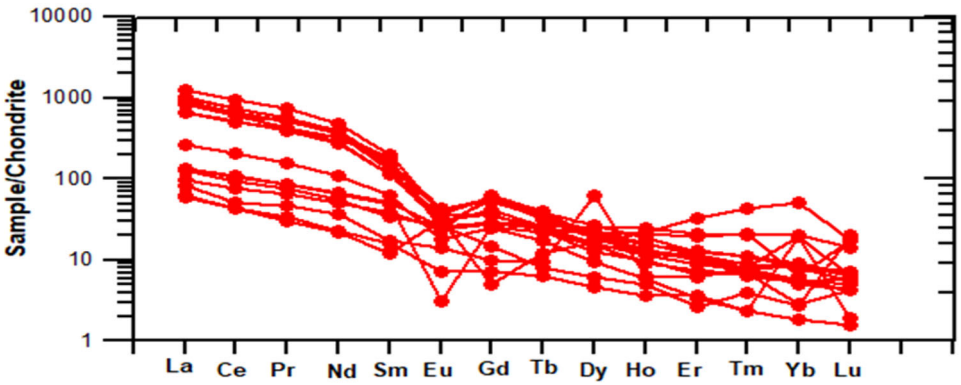

Fig. 6 Chondrite-normalized REE diagram for the granitic rocks (values from Sun and McDonough 1991)

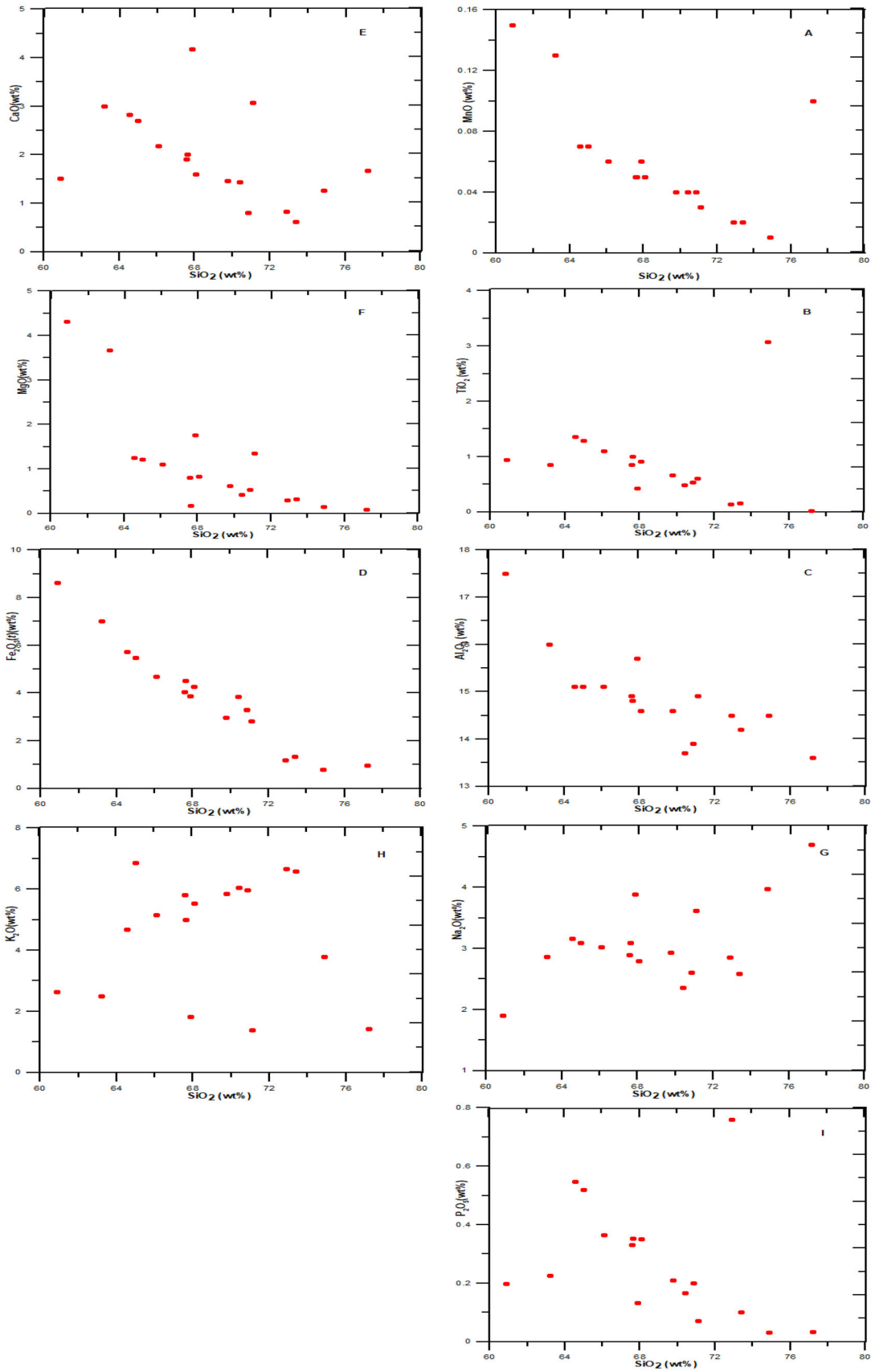
E
CaO(wt%)
SiO2 (wt%)
A
MnO (wt%)
SiO2 (wt%)
F
MgO(wt%)
SiO2 (wt%)
B
TiO2 (wt%)
SiO2 (wt%)
D
Fe2O3(t)(wt%)
SiO2 (wt%)
C
Al2O3 (wt%)
SiO2 (wt%)
H
K2O(wt%)
SiO2 (wt%)
G
Na2O(wt%)
SiO2 (wt%)
I
P2O5(wt%)
SiO2 (wt%)

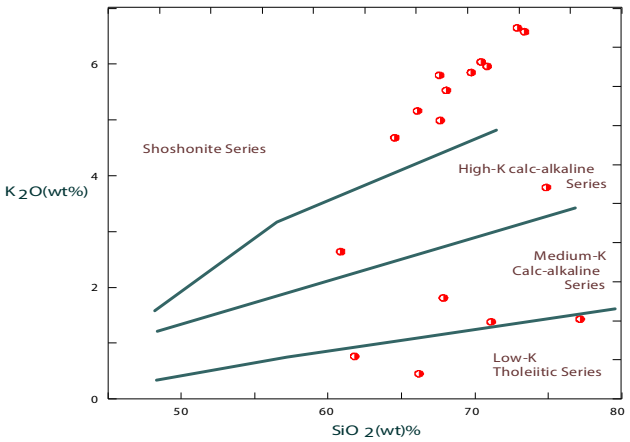

Fig. 8 Harker variation diagram for the granitic intrusions in the study area

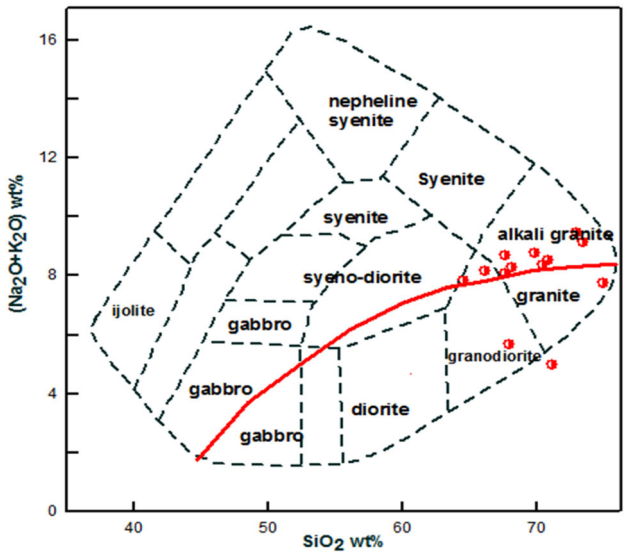

Fig. 9 Subdivision of subalkaline rocks using the K_2O versus SiO_2 diagram after (Le Maître et al. 1989)

The data on the granitic rocks were also plotted in the modified alkali-lime index (MALI) ($Na_2O + K_2O$–CaO) versus silica (SiO_2) and the Fe* index [$FeO^{tot}/(FeO^{tot} + MgO)$] versus silica ($SiO_2$) (wt%) diagrams (Figs. 10, 11) of Frost et al. (2001). In the MALI–SiO_2 diagram, the data points lie in the alkali-calcic to the calcic region, lying mainly in the I & S-type field while in the Fe* index versus SiO_2 diagram, the data plot mostly as ferroan, with a few as magnesian. The pegmatite is classified as LCT according to Cerny and Ercit (2005). They are enriched in lithium, cesium, and tantalum. Most of the pegmatites with the LCT signature have a compositional affinity with S-type granites (Chappell and White 2001).

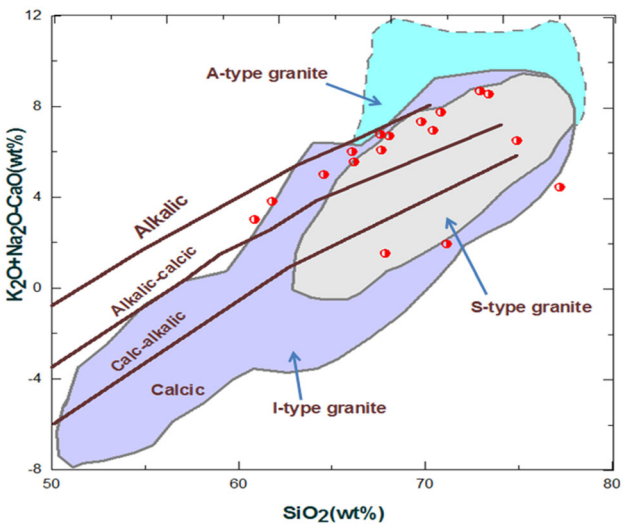

Fig. 10 Binary plot of molecular ratio of alumina to alkalis [$Al_2O_3/(Na_2O + K_2O)$] versus alumina to lime and alkalis [$Al_2O_3/(CaO + Na_2O + K_2O)$] classifying the granitic rocks in the study area as peraluminous (after Shand 1943)

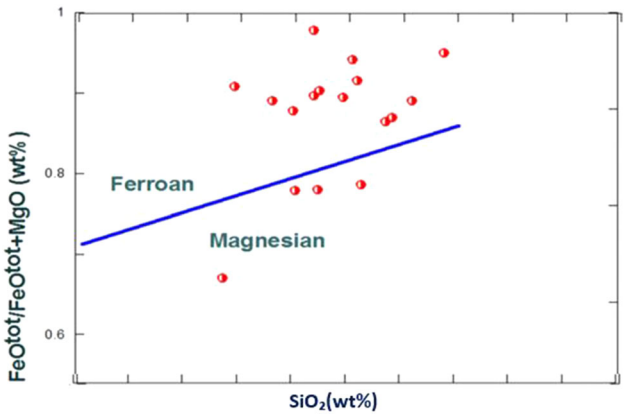

Fig. 11 Plots of the granitic rocks on the modified Alkali-Lime Index (MALI) versus Silica (SiO_2) diagram, with SIAM Classification (after Frost et al. 2001)

According to Chappell (1999), a metasedimentary source will usually produce magmas with low alkali contents and high alumina, exhibiting peraluminous character.

Most of the granitic rocks plot in the field of mafic pelites, but two samples of the weakly foliated leucogranodiorite plot in the field of the felsic pelites on the Patiño-Douce and Beard (1995) diagram for discrimination of the sources of granitic rocks, showing affinity to the low pressure (< 4 Kb) conditions (Fig. 13).

The trace element data are also plotted on conventional Harker-type variation diagram (Fig. 14), and the granitic rocks show typical calc-alkaline trends with Nb, Zr, La, Ba, and Sr generally decreasing and Rb increasing with increasing SiO_2.

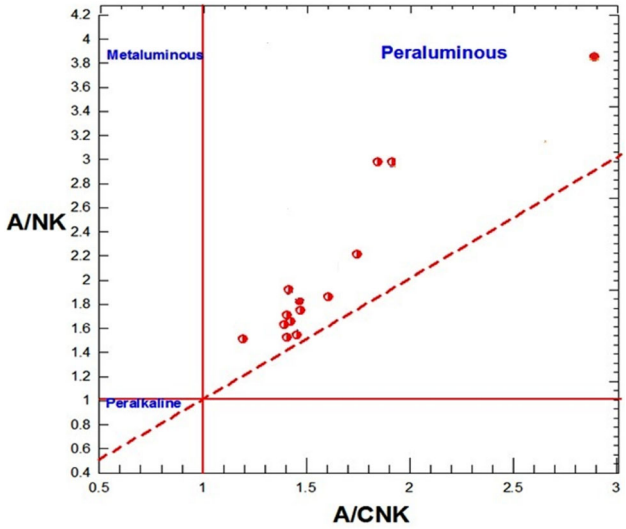

Fig. 12 FeOt/(FeOt + MgO) versus SiO_2 (wt%) (after Frost et al. 2001)

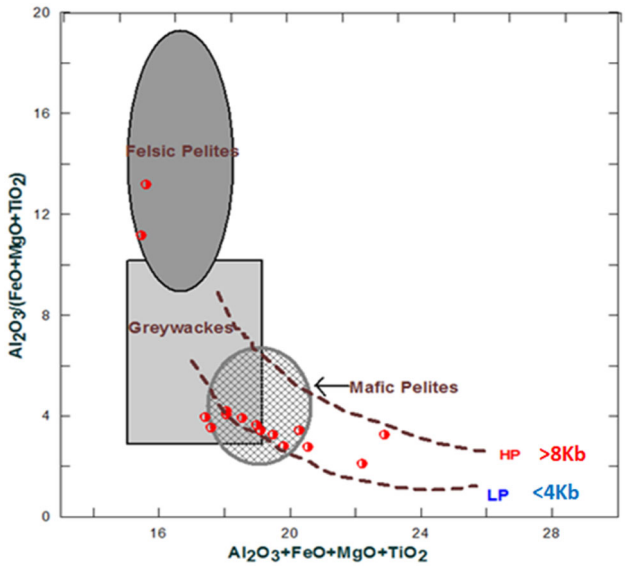

Fig. 13 Discrimination diagram of $Al_2O_3/(FeO + MgO + TiO_2)$ versus $Al_2O_3 + FeO + MgO + TiO_2$ of Patiño-Douce (1999) for the different sources of granitic rocks

From trace and rare earth elements data, the depletion in Ti, Nb, Ta, and Sr and the enrichment in the LILE (Rb, K and Th) of the rocks suggest a crustal source. According to Harris et al. (1986) and Chappell and White (1992), high Rb, K, and Th and low P, Sr, and Ti values are compatible with typical crustal melts and suggest evolution from partial melting of crustal materials. Plots of MgO versus FeOt in a diagram (Fig. 15) after Zorpi et al. (1989) further suggest that partial melting was a major mechanism for the formation of the granitoids.

The moderate to high fractionations with pronounced negative Eu anomalies shown in the REE pattern for the granitic rocks is typical behavior of crustal-generated granites and suggest either the fractionation of plagioclase or its retention of the source in the case of partial melting (Frost et al. 2001). The similarity of the REE patterns of the granitic rocks suggests that they are co-genetic. The light REE enrichment relative to the heavy REE enrichment in the rocks in this study is considered as an indicator of varying degrees of partial melting. The negative Eu anomaly shown by the granitic rocks suggests either the fractionation of plagioclase or its retention in the source in the case of partial melting. The REE patterns for the granites show moderate to high fractionation with pronounced negative Eu anomaly, which is typical behavior of crustally-generated granites. The rocks are characterized by widespread contamination and preferential incorporation of low-melting components including K_2O through assimilative reaction with the K-rich metasediment rocks. This could be responsible for K_2O enrichment in the rocks.

The peraluminous character of the granitic rocks in this study is consistent with the findings of other researchers of the Nigerian Basement Complex. Rahman et al. (1988) reported that granitic rocks around Oban Massif, southeastern Nigeria are peraluminous. The granitic gneisses of Aderan area are calc-alkaline and peraluminous granites emplaced during the Pan-African orogeny (Okonkwo and Folorunso 2013). They are different from granitic rocks in Igbeti (SW Nigeria) (Rahman et al. 1988), Ityowanye, and Katsina-Ala areas (SE Nigeria) (Obiora 2012) that are metaluminous.

The Older granites in northern and southwestern Nigeria Basement contain a significant amount of alkali and are peraluminous with corundum appearing in the norm (Odeyemi 1977; Olanrewaju and Rahaman 1982). Also, granitic gneiss around Jebba area (SW Nigeria) are peraluminous (Okonkwo and Ganev 2012). The strongly peraluminous nature of the rocks is very likely to be a reflection of derivation from partial melting of pelitic or semi-pelitic gneisses during the high-grade regional metamorphism that affected the area. The possibility of derivation of peraluminous melts from hydrous melting of pelitic or semi-pelitic rocks is supported by Frost et al. (2001), as well as Obiora and Ukaegbu (2008). The shoshonitic, alkali-calcic and peraluminous character of the granitic rocks make them similar to the Caledonian granitoids of Ireland and Britain (Frost et al. 2001), more

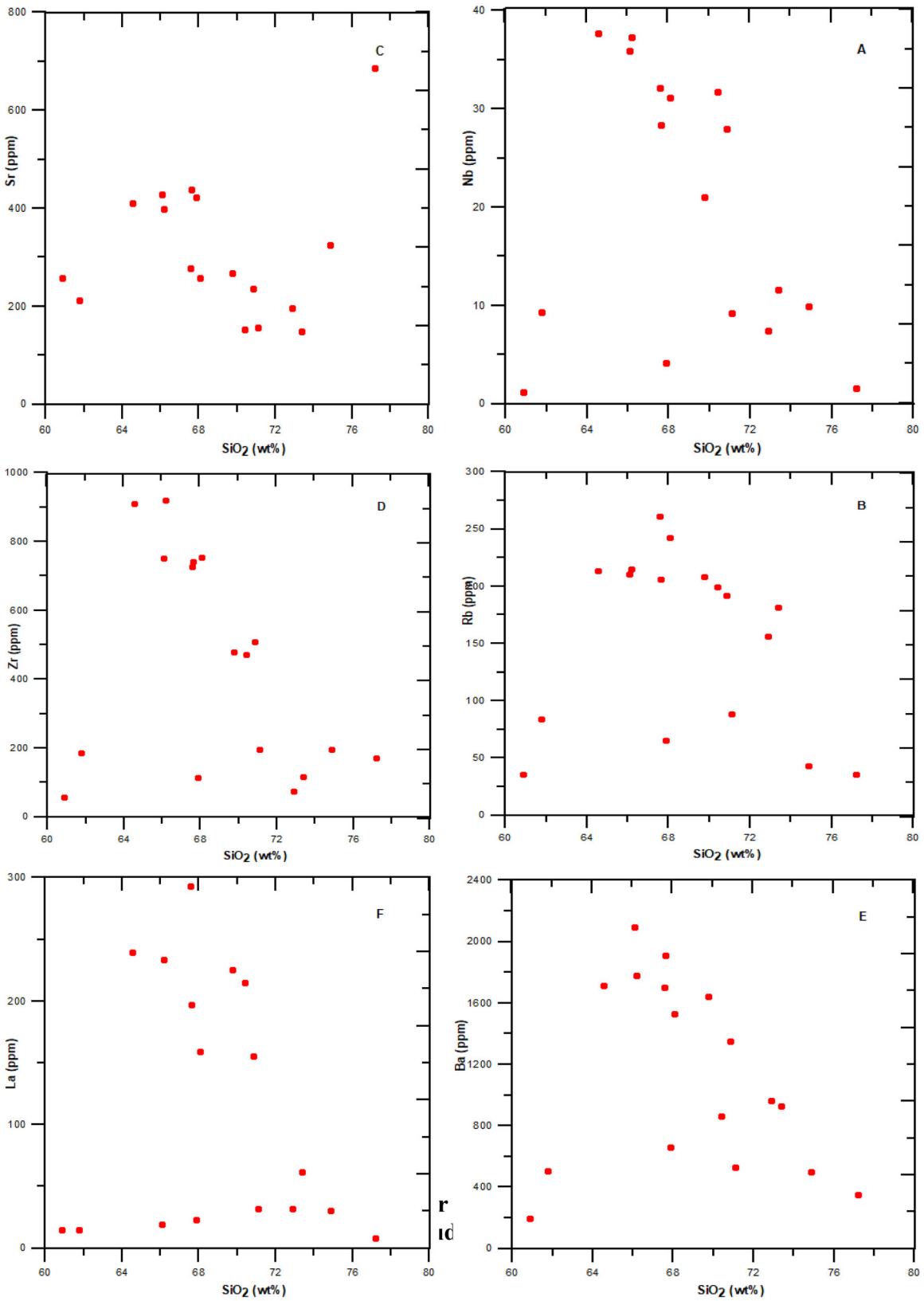

Fig. 14 Plot of Zr, Rb, Sr, Nb, La and Ba against SiO_2

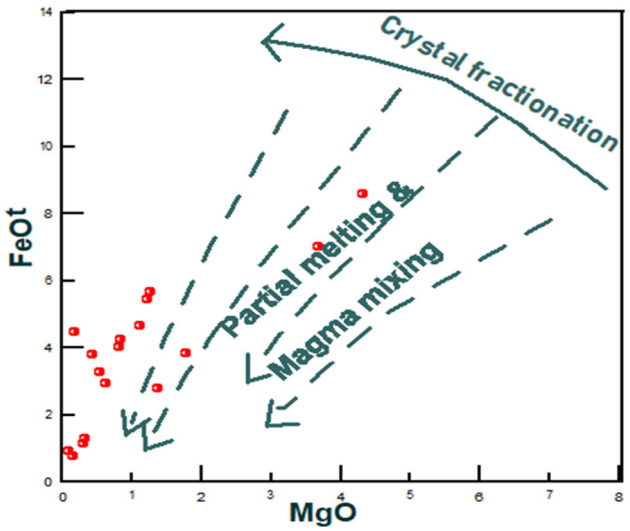

Fig. 15 FeO versus MgO diagram (after Zorpi et al. 1989)

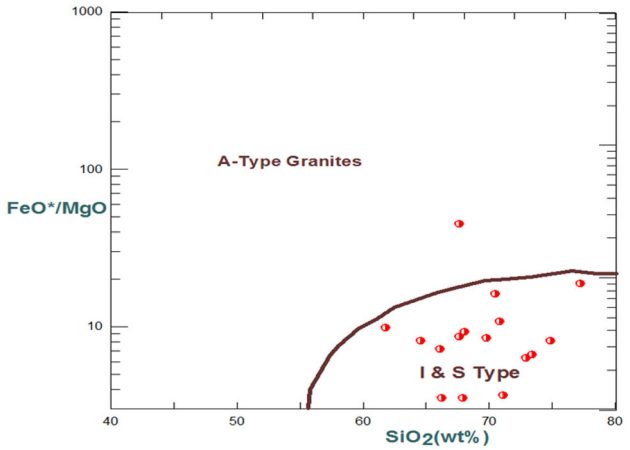

Fig. 16 SIAM Classification (FeO*/MgO vs. SiO_2) (wt%) diagram for the granitic rocks (after Chappell and White 1974)

commonly referred to as post-orogenic granitoids, shoshonitic granitoids, and K-rich calc-alkaline granitoids.

6.2 Tectonic setting of the granitic rocks

In the FeO*/MgO versus SiO_2 diagram of Chappell and White (1974) (Fig. 16), the granitic rocks fall within the I and S type fields correlating positively with the Himalayan-type granite. S-type granites originate by melting or ultrametamorphism of pre-existing metasedimentary or sedimentary rocks (containing Al, Na, and K oxides and are said to be peraluminous) observable in deeply eroded cores of fold-thrust mountain belts formed as a result of continent–continent collisions, and are thus orogenic granites (Chappell and White 1974).

Numerous studies had recommended that trace elements be used to discriminate between the different tectonic settings of granitoid magmas (Pearce et al. 1984; Harris et al. 1986). Zhou et al. (2014) were of the opinion that they must be used with caution, as they could represent the formation of the protoliths, rather than those of the derived magma.

The granitic rocks in the study area plot within the post-collisional (Post-COLG) field on the Rb versus Y + Nb tectonic discrimination diagram after Pearce et al. (1984) (Fig. 17), which suggests that they could be formed in a compressional setting. The granitic rocks in this study are quite similar to those of the Pan-African (Older) granitic rocks rather than the Jurassic (younger) granites in terms of their geochemical characteristics. From the analysis for tectonic setting of the rocks using geochemical discrimination diagrams, the rocks are seen to be related to Pan African granites, otherwise known as the Older granites which were emplaced towards the end of the Pan African orogeny (600 Ma), during the collision of the West African craton and the Tuareg shield Obiora (2012). Table 4 shows a compilation of age data of the Pan African (Older) granites in Nigeria.

The overall geochemical features of the granitic rocks indicate that they were most likely derived from partial melting of crustal materials in an orogenic (post-collisional) tectonic setting. They are therefore related to the Pan-African granites, otherwise known as the Older

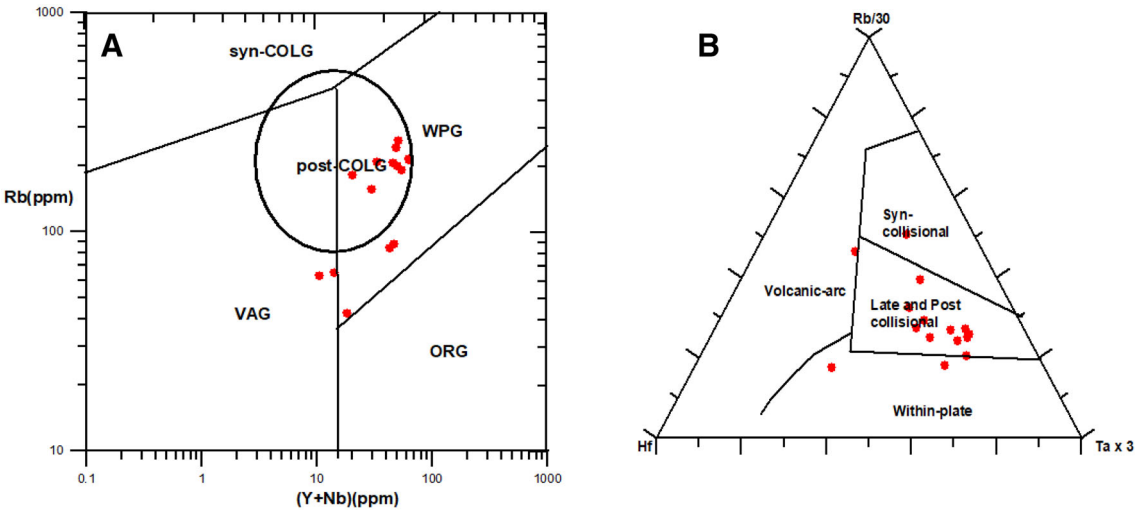

Fig. 17 **a** Post orogenic character of the granitoids shown on the Rb versus Y + Nb of Pearce et al. (1984). *Syn-COLG* syn-collision granites, *post-COLG* post-collision granites, *WPG* within plate granites, *VAG* volcanic arc granites, *ORG* ocean ridge granites. **b** Plots of the rocks in the fields of Syn-collisional to Late/post-collisional granitoids on the Rb/30 Hf (Ta ×3) diagram of Harris et al. (1986)

Granites which were emplaced during the Pan African orogenic event.

Acknowledgements The authors are grateful to the University of Nigeria, Nsukka for employing the first author as a graduate assistant who made the study possible. The assistance of the Association of Applied Geochemists (AAG) in carrying out the whole rock geochemical analyses (In-Kind Analytical support) is greatly acknowledged. They are also grateful to the Tertiary Education Trust Fund (IBR-2017) for sponsoring the field work and petrographic analysis.

References

Akoh JU, Ogunleye PO, Aliyu AI (2015) Geochemical evolution of micas and Sn-, Nb-, Ta-mineralization associated with the rare metal pegmatite in Angwan Doka, central Nigeria. J Afr Earth Sc 97:167–174

Black R, Caby R, Moussine-Pouchkine A, Bertrand JM, Fabre J, Lesquer A (1979) Evidence for the Late Precambrian plate tectonics in West Africa. Nature 278:223–227

Burke KC, Dewey JF (1972) Orogeny in Africa. In: Dessauvagie TFJ, Whiteman AJ (eds) Africa geology. University of Ibadan Press, Ibadan, pp 583–608

Caby R, Bertrand JML, Black R (1981) Pan-African ocean closure and continental collision in the Hoggar-Iforas segment, Central Sahara. In: Kroner A (ed) Precambrian plate tectonics. Elsevier, Amsterdam, pp 407–434

Caen-Vachette M, Umeji AC (1983) Whole-rock Rb–Sr dating of two Monzogranites in Southern Nigeria and their implications on the age of the Pan-African orogenic cycle. J Afr Earth Sci 1:339–342

Cerny P, Ercit TS (2005) The classification of granitic pegmatites revised. Can Mineral 43(6):2005–2026

Chappell BW (1999) Aluminium saturation in I and S-type granites and the characterization of fractionated haplogranites. Lithos 46:535–551

Chappell BW, White AJR (1974) Two contrasting granite types. Pac J 8:173–174

Chappell BW, White AJR (1992) I- and S-type granites in the Lachlan fold belt. In: Brown PE, Chappell BW (ed) The second Hutton symposium on the origin of granites and related rocks. Edinburgh Earth. Sciences, vol 83, pp 1–26

Chappell BW, White AJR (2001) Two contrasting granite types: 25 years later. Austral J Ear Sci 48:489–499

Cox KG, Bell JD, Pankhurst RJ (1979) The interpretation of igneous rocks. Allen and Unwin, London

Dada SS, Respaut JP (1989) The quartz fayalite monzonite (bauchite) of Bauchi, new evidence of a syntectonic Pan-African magmatism in northern Nigeria. C R Acad Sci 309:887–892

Dada SS, Briqueu L, Harms U, Lancelot JR, Matheis G (1995) Charnockitic and monzonitic Pan-African series from north-central Nigeria: trace-element and Nd, Sr, Pd isotope constraints on their petrogenesis. Chem Geol 124:233–252

Ekwueme BN (1987) Structural orientations and Precambrian deformation episodes of Uwet area, Oban massif, Southeastern Nigeria. Precambr Res 34:269–289

Ekwueme BN (1994) Structural features of Obudu Plateau, Bamenda Massif, Eastern Nigeria: preliminary interpretation. J Min Geol 30(1):45–59

Ferre EC, Caby R, Peucat JJ, Capdevila IR, Monie P (1998) Pan-African post-collisional, ferropotassic granite and quartz-monzonite plutons of Eastern Nigeria. Lithos 45:255–278

Ferre EC, Gleizes G, Caby R (2002) Obliquely convergent tectonics and granite emplacement in the Trans-Saharan belt of Eastern Nigeria: a synthesis. Precambr Res 114:199–219

Frost BR, Barnes CG, Collins WJ, Arculus RJ, Ellis DJ, Frost CD (2001) A geochemical classification for granitic rocks. J Petrol 42:2033–2048

Grant NK (1978) Structural distinction between metasedimentary cover and underlying basement in 600 M.Y. old Pan-African domain. Geol Soc Bull 89:50–58

Harris NBW, Pearce JA, Tindle AG (1986) Geochemical characteristics of collision-zone magmatism. In: Coward MP, Reis AC (eds) Collision tectonics. Special publication, vol 19. Geological Society, London, pp 67–81

Jones HA, Hockey RD (1964) The geology of part of southwestern Nigeria. Niger Geol Surv Bull 31:87

Khalaji AA (2007) Petrology and geochemistry of the granitoid complex of Boroujerd, Sanandaj-Sirjan Zone, Western Iran. J Asian Earth Sci 144:56–76

Leblanc M (1981) The Late Proterozoic ophiolites of BouAzzer (Morocco): evidence for Pan-African plate tectonics. In: Kroner A (ed) Precambrian plate tectonics. Elsevier, Amsterdam, pp 435–451

Le Maitre RW, Bateman P, Dudek AJ, Keller MJ (1989) A Classification of Igneous Rocks and Glossary of Terms. Blackwell, Oxford, p 193

Makanjuola AA (1982) A review of the petrology of the Nigerian syenites. J Min Geol 19:1–14

McCurry P, Wright JB (1977) On place and time in orogenic granite plutonism. J Geol Soc Am 82(6):1713–1716

Nigerian Geological Survey Agency (1994) Geological map of Nigeria

Nigerian Geological Survey Agency (2004) Geological map of Nigeria

Nigerian Geological Survey Agency (2011) Geological map of Nigeria

Obiora SC (2005) Field descriptions of hard rocks, with examples from the Nigerian Basement Complex. SNAAP Press (Nig.) Ltd., Enugu

Obiora SC (2006) Petrology and geotectonic setting of the Basement Complex rocks around Ogoja, Southeastern Nigeria. Ghana J Sci 46:13–46

Obiora SC (2012) Chemical characterization and tectonic evolution of hornblende-biotite granitoids from the Precambrian Basement Complex around Ityowanye and Katsina-Ala, Southeastern Nigeria. J Min Geol 48(1):13–29

Obiora SC, Ukaegbu VU (2008) Petrology and geochemical characteristics of Precambrian granitic basement complex rocks in the southernmost part of North-Central Nigeria. Chin J Geochem 28:377–385

Odeyemi IB (1977) On the petrology of the basement rocks around Igarra, Bendel state, Nigeria. Unpublished Ph.D. thesis, University of Ibadan

Okonkwo CT, Folorunso IO (2013) Petrochemistry and geotectonic setting of granitic rocks in Aderan area, S.W. Nigeria. J Geogr Geol 5(1):30

Okonkwo CT, Ganev VY (2012) U-Pb geochronology of the Jebba granitic gneiss and its implications for the paleoproterozoic evolution of Jebba area, Southwestern Nigeria. Int J Geosci 3:1065–1073

Olarewaju VO (1987) Charnockite-granite association in SW Nigeria: Rapakivi granite type and charnockite plutonism in Nigeria. J Afr Earth Sc 6:67–77

Olanrewaju VO, Rahaman MA (1982) Petrology and Geochemistry of the Older Granites from some parts of Northern Nigeria. J Min Geol 17:2

Oyawoye MO (1964) The geology of the Nigerian Basement Complex—a survey of our present knowledge of them. J Niger Metall Soc 1(2):87–102

Oyawoye MO (1970) The basement complex of Nigeria. Afr Geol 1:67–99

Patiño-Douce AE (1999) Generation of metaluminous A-type granites by low pressure melting of calc-alkaline granitoids. Geology 25:743–746

Patiño-Douce AA, Beard JS (1995) Dehydration-melting of biotite gneiss and quartz amphibolite from 3 to 15 kbar. J Petrol 36:707–738

Pearce JA, Harris NBW, Tindle AG (1984) Trace element discrimination diagram for the tectonic interpretation of granitic rocks. J Petrol 25(4):956–983

Rahaman MA (1976) Review of the basement geology of Southwestern Nigeria. In: Kogbe CA (ed) Geology of Nigeria. Elizabethan Publication Company, Lagos, pp 41–58

Rahaman MA (1989) Review of the basement geology of southwestern Nigeria. In: Kogbe CA (ed) Geology of Nigeria, 2nd edn. Rock View Publication Company, Jos, pp 39–56

Rahman AMS, Ekwere SJ, Azmatullah M, Ukpong EE (1988) Petrology and geochemistry of granitic intrusive rocks from the western part of Oban Massif, Southeastern Nigeria. J Afr Earth Sci 7:149–157

Shand SJ (1943) Eruptive rocks: their genesis, composition, classification, and their relation to ore-deposits with a chapter on meteorite. Wiley, New York

Strekeisen A (1976) To each plutonic rock, its proper name. Earth Sci Rev 12:1–33

Sun SS, McDonough WF (1991) Chemical and isotopic systematic of oceanic basalts: implication for mantle composition and processes. In: Sunders AD, Norry MJ (eds) Magmatic in oceanic basins. Special publication, vol 42. Geology Society of London, London, pp 313–345

Thompson RN (1982) British Tertiary volcanic province. Scott J Geol 18:49–67

Wilson M (1989) Igneous petrogenesis. Unwin Hyman, London

Zhou YY, Zhai MG, Zhao TP, Lan ZW, Sun QY (2014) Geochronological and geochemical constraints on the petrogenesis of the early Paleoproterozoic potassic granite in the Lushan area, southern margin of the North China Craton. J Asian Earth Sci 94:190–204

Zorpi MJ, Coulon C, Orsini JB, Cocirta C (1989) Magma mingling, zoning and emplacement in calc-alkaline granitoid plutons. Tectonophysics 157:315–329